Structures and Vibrational Frequencies of the Quinones in *Rb. sphaeroides* Derived by a Combined Density Functional/Molecular Mechanics Approach

Marco Nonella, Gerald Mathias, Markus Eichinger, and Paul Tavan*

Theoretische Biophysik, Lehrstuhl für BioMolekulare Optik, Ludwig-Maximilians Universität München, Oettingenstrasse 67, D-80538 München, Germany

Received: August 21, 2002; In Final Form: October 29, 2002

The structures of the ubiquinones Q_A and Q_B in the bacterial photosynthetic reaction center of *Rhodobacter sphaeroides* are calculated by a quantum mechanical/molecular mechanics hybrid technique. The orientations of their methoxy groups are found to differ by less than 30°. Calculation of the vibrational spectra reveals that one C═O stretching mode of Q_A is considerably shifted to lower frequencies in agreement with the experimental data. The orientational differences of the methoxy groups at Q_A and Q_B are too small as to provide an explanation for this shift. Instead, it must be due to a very special interaction of the protein with Q_A. Artificial neutralization of the iron cofactor, while keeping all other structural parameters of the reaction center fixed, reveals that this interaction arises from the electrostatic field of the Fe^{2+} ion, within which Q_A is oriented in a particular way.

1. Introduction

Quinones play important parts in the redox reactions occurring in respiration and photosynthesis.[1] Bacterial photosynthetic reaction centers (RCs), for example, have two quinones carrying out different functions. After light-induced charge separation at the so-called "special pair" of bacteriochlorophyll molecules, the primary quinone Q_A accepts an electron and transfers it to the secondary quinone Q_B. When Q_B has taken up two electrons and two protons, it leaves the RC as a dihydroquinone Q_BH_2, diffuses across the membrane, deposits the electrons at a cytochrome and the protons into the solvent as to complete the vectorial transmembrane proton transport, which in photosynthesis represents the primary step of light−energy conversion and is coupled to an electron transport cycle here.[2]

In the bacterial photosynthetic RC of *Rhodobacter sphaeroides*, the two quinones are both ubiquinones (2,3-dimethoxy-5-polyprenyl-6-methyl-1,4-benzoquinone). Figure 1 shows part of the X-ray structure 1PCR[3] of this protein including the ubiquinones, the iron cofactor, several amino acids, and water molecules. The different functions of the quinones are reflected by different spectroscopic and thermodynamic properties. Whereas the carbonyl stretching modes of Q_B absorb at 1641 cm^{-1},[4] which is 10−20 cm^{-1} to the red of the corresponding absorption in solution, one carbonyl mode of Q_A is much more strongly red-shifted to 1601 cm^{-1}.[5,6] Experiments with isotopically labeled quinones have shown that the shifted C═O mode is localized at the bond C_4═O,[5,6] which, therefore, has been marked in Figure 1. Furthermore, the redox potentials of the two quinones differ by about 70 mV.[7,8]

The different properties of Q_A and Q_B could either be caused by different orientations of the methoxy groups at the two sites[5,9] or by other quinone−protein interactions.[5,10] Indeed, various computational studies on isolated quinone model compounds have made clear that the orientations of the methoxy groups can affect the vibrational frequencies[9,11] and the redox potential.[9,12−14] It has therefore been suggested that proteins might tune the redox properties of ubiquinones by steering the orientations of the methoxy groups.[12] For a ubiquinone model compound, Figure 2 illustrates the two torsional degrees of freedom, whose variation couples to the molecular properties. However, calculations on simple quinone−water or quinone−cation model complexes have shown that electrostatic interactions can modify the torsional potentials of the methoxy groups and, hence, the relation between methoxy orientation and redox properties. They can also change the vibrational frequencies of the carbonyl bonds. In particular, the interaction with a positively

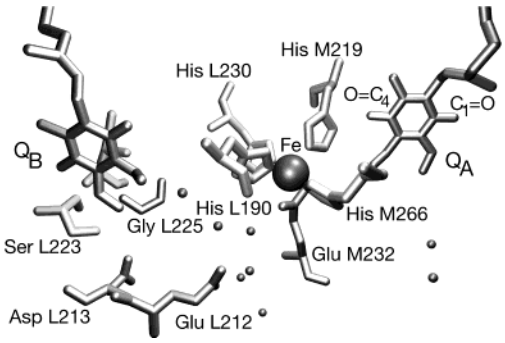

Figure 1. Quinones QA and QB in the RC of *Rb. sphaeroides*.

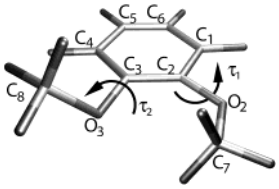

Figure 2. 2,3-Dimethoxy-1,4-benzoquinone containing different substituents at C5 and C6 has served as a vacuum model for the ubiquinones of *Rb. sphaeroides* in previous computational studies quoted in the text. The orientations of the methoxy groups can be measured by the dihedral angles C7−O2−C2−C3 and C8−O3−C3−C2, which we call τ_1 and τ_2, respectively. In ubiquinone, the isoprene chain is attached to C6.

* To whom correspondence should be addressed. E-mail: tavan@physik.uni-muenchen.de.

10.1021/jp026810+ CCC: $25.00
Published on Web 12/07/2002

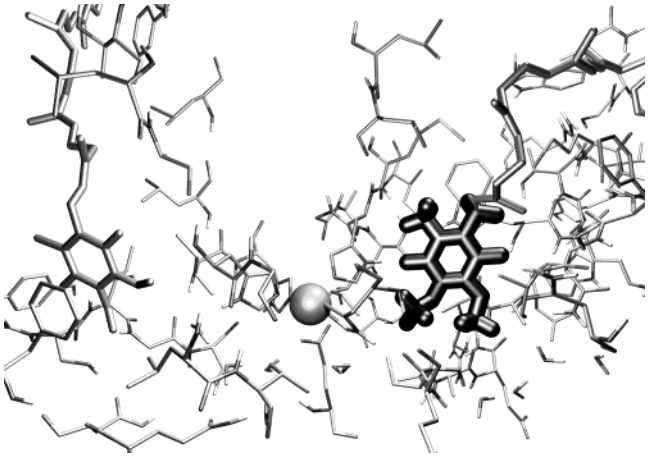

Figure 3. Decomposition of the RC of *Rb. sphaeroides* into a QM fragment drawn in black and an MM fragment drawn in gray. Only a small part of the whole protein has been selected for viewing. The choice includes the quinones and the iron cofactor. The shown decomposition is adequate for an in situ QM calculation of the properties of QA.

charged ion has been predicted to cause a large red shift of the C═O mode pointing toward this ion.[15] Therefore, the question, whether steric or electrostatic interactions provide the mechanism, by which the RC of *Rb. sphaeroides* selectively tunes the properties of Q_A and Q_B, remained open up to now.

In this paper, we want to address this question by a novel computational approach,[16,17] which should be capable of providing a definite answer, since it has been designed to describe the vibrational spectra of molecules in condensed phase at a high precision. This approach allows us to combine an accurate quantum mechanical (QM) description of a quinone, which then makes up the so-called QM fragment of the simulation system, with a sufficiently accurate microscopic molecular mechanics (MM) model of the surrounding protein, which is collected into the remaining MM fragment.

The basic concepts of such QM/MM hybrid methods have been introduced in the pioneering work of Warshel and Levitt.[18] Only recently, however, their accuracy has reached a stage, which makes them suitable for quantitative computation of vibrational spectra in condensed phase. Here, the key progress has been the use of density functional methods (DFT)[19,20] for the QM part.[16,17,21−26]

Figure 3 illustrates a QM/MM decomposition for the given protein and, in particular, for a DFT calculation of the properties of Q_A in its native protein environment. For the QM fragment, our computational approach[16,17] uses DFT as implemented in the program package CPMD[27] and for the MM fragment a force field, which explicitly accounts for the long-range electrostatics of the protein and solvent through structure-adapted multipole expansions (SAMM).[28−31] The MM force field and an interface to CPMD are implemented in our molecular dynamics (MD) program EGO/MMII.

For the vibrational analysis of molecules in the gas phase, the development[19,20] and widespread accessibility[32] of DFT have been a breakthrough (see, e.g., ref 33). In particular, for the intramolecular force field of the smallest quinone compound, i.e., 1,4-benzoquinone, the validity of DFT descriptions has been demonstrated already in 1995.[34] Here, the gradient-corrected exchange functional of Becke[35] and the correlation functional of Perdew[36] together with a Gaussian 6-31G** basis set[37] (denoted as BP86/6-31G**) have been shown to yield harmonic frequencies for the C═O and C═C modes, which quantitatively reproduce gas phase observations and, therefore, render scaling procedures superfluous.

Meanwhile, a variety of DFT methods have been applied to the prediction of quinone structures and vibrational spectra[11,38−41] including methoxy-substituted quinones and, here particularly, 2,3-dimethoxy quinones as depicted in Figure 2. The vacuum calculations on the structure of such ubiquinone models have rendered partially conflicting results. The differences of results are mainly due to the shallow torsional potentials of the methoxy groups, whose accurate description poses a challenge to computational methods. However, because experimental evidence on the gas phase structure of this model compound is lacking, a detailed evaluation of the various approaches is impossible. Therefore, in this respect, one has to rely on the quoted benzoquinone study,[34] which has singled out BP86/6-31G** as a most accurate DFT approach for this class of compounds.

Unfortunately, the DFT module CPMD of our QM/MM hybrid program does not provide exactly this method but solely related procedures. It employs plane wave expansions instead of atom-centered Gaussians as basis sets for the Kohn−Sham MOs and applies the frozen core approximation as described by pseudopotentials instead of an all-electron treatment. These differences make a comparison of CPMD with BP86/6-31G** descriptions necessary, if one wants to get an estimate on the accuracy of the DFT methods provided by CPMD. As a test case serving for the selection and the calibration of the DFT approaches provided by CPMD, we will therefore have to carry out vacuum calculations on 1,4-benzoquinone, before we can turn to studies of condensed phase phenomena.

Once a DFT description provided by CPMD has been selected, which can render gas phase descriptions of quinone compounds at a given accuracy, one may expect from the arguments and test calculations given in refs 16 and 17 that the transition to the condensed phase by application of the corresponding QM/MM hybrid method will hardly deteriorate the accuracy of the DFT results. In particular, we expect that the MM models of the environment and of its interaction with the QM fragment are good enough as to render for that fragment high-quality vibrational spectra. In line with our aim of differentiating the properties of Q_A and Q_B, we will select these quinones as the respective QM fragments for our hybrid calculations. Concerning the evaluation of computational methods, it will be interesting to see whether the applied QM/MM approach actually matches the expectations voiced above. However, this methodological question solely represents a (although important) side aspect of this study. Its central aim is an answer to the question, why Q_A and Q_B exhibit the observed differences and how the RC of *Rb. sphaeroides* steers their properties.

2. Computational Methods and Setup of the Simulation System

As mentioned above, the calculations are carried out with a QM/MM hybrid method, which is described in detail in refs 16 and 17 and is implemented in a combination of the MM MD program EGO/MMII[31] with the DFT program CPMD.[27] Because CPMD uses plane wave basis sets and pseudopotentials, a particular DFT method is defined here by the type of exchange−correlation functional, by the chosen pseudopotential, and by the cutoff energy for the basis set. We have tested three such methods for the description of quinones: First, we have selected the gradient-corrected exchange functional of Becke[35] and the correlation functional of Perdew,[36] since this choice of func-

tionals had been successful for a Gaussian basis (BP86/6-31G**) in the case of benzoquinone as discussed further above. Large basis sets characterized by a cutoff at 70 Ry are required, if these functionals are combined with the normconserving pseudopotentials of Troullier and Martins.[42] We will denote this CPMD method by MT/BP. A second similarly expensive approach, denoted by MT/BLYP, is obtained, if Perdew's correlation functional is replaced by the one of Lee, Yang, and Parr.[43] A computationally much cheaper, but not necessarily very accurate method, in which a cutoff at 25 Ry suffices,[44] combines the supersoft Vanderbilt pseudopotentials[45] with the local density approximation.[46] We refer to this method as VDB/LDA.

The description of the MM fragment by EGO/MMII is compatible with most standard force fields for protein−solvent systems. In this study, we have used the united atom model provided by the CHARMM force field.[47] Parameters for chemical compounds not contained in this library have been adopted from refs 48−51. Because of the use of the SAMM algorithm,[28,29] no cutoff is applied to the electrostatics.

QM/MM hybrid simulations require a careful setup of the simulation system and, subsequently, the design of computational procedures, which enable accurate calculations of the desired observables. Our simulation system, which serves to calculate the quinone vibrational spectra in *Rb. sphaeroides*, has the 2.65 Å resolution crystal structure 1PCR of Ermler et al.[3] as its starting point. To create from such a structure a suitable QM/MM simulation system, a series of modeling steps have to be executed addressing the following problems: (i) X-ray structures usually do not cover all atoms actually present in a protein; in particular, all hydrogen atoms are absent; thus, one has to add missing atoms. (ii) The electrostatic shielding by the solvent has to be taken into account. (iii) For titratable groups buried in the interior of the protein, the protonation states have to be determined as to obtain a correct charge distribution in this low-dielectric medium. (iv) The system has to be partitioned into QM and MM fragments.

As far as point (i) is concerned, the isoprene chains of the two ubiquinones in the crystal structure contain only seven units instead of the required 10. Because it has been shown by Fourier transform infrared (FTIR) spectroscopy that only the first isoprene unit does affect quinone binding,[6] we have left out the missing units. Furthermore, the authors of the 1PCR structure speculate that additional water molecules are present near Q_B, which are not seen in the electron density at the given resolution. We did not try to complete the structure in this respect. Finally, because we have chosen a united atom model for the protein, we had to add only the polar hydrogen atoms. A tool managing this task is provided by the program X-PLOR.[52]

For point (ii), the best solution would be to embed the RC into a large membrane/solvent system. However, because we are solely interested in the properties of the quinones, which are located in the trans-membrane part of the protein, we decided to avoid a costly explicit solvent model. Instead, we have neutralized those ionic amino acids, which are accessible by the solvent, to model their shielding by the high dielectric and by the ions of the solvent.[17] Test calculations have shown that ionizing these residues shifts the quinone vibrational frequencies by less than 10 cm^{-1}. This worst case scenario assumes no shielding at all for the ionic groups exposed to the solvent. Because of the well-known effectivity of solvent shielding, we expect, however, that the errors of our crude solvent model are by an order of magnitude smaller than the quoted worst case estimate.

The question of protonation states raised in point (iii) is nontrivial, particularly since p*K* calculations are notoriously unreliable and since experimental evidence is hard to obtain. In the dark-adapted state mapped by the chosen X-ray structure 1PCR[3], there are two acidic groups (Glu L212 and Asp L213) in the close vicinity of Q_B (cf. Figure 1), which occupies the so-called distal binding site.[3,53] The protonation states of these acids are under debate. Paddock et al.[54] concluded from experiments with mutated RCs that Glu L212 is protonated and Asp L213 is ionized. This conclusion agrees with results of p*K* calculations[55,56] but is at variance with FTIR observations on mutated RCs,[57] according to which both acids should be ionized. It is also at variance with a MD study, in which the distal binding site has been found unstable, if Glu L212 is protonated and Asp L213 is ionized.[58] On the other hand, electrostatics calculations by Sham et al.,[59,60] which properly include protein relaxation, have predicted that both Glu L212 and Asp L213 are ionized in the 1PCR structure. Because of these uncertainties, we have initially chosen both groups to be protonated and have studied the effects of ionization on the vibrations of Q_B (cf. Section 3.2). In agreement with observations,[61] we have neutralized Glu L104.

The chosen partition of the simulation system into QM and MM fragments required by point (iv) is illustrated by Figure 3 for Q_A. Apparently, the partition of the RC into fragments cuts also the isoprene chain of Q_A, for which purpose the link atom method developed in refs 16 and 17 has been applied. For Q_B, we have employed an analogous partitioning.

Having thus described the setup of the simulation system, we still have to sketch the sequence of computational procedures serving to calculate the quinone vibrational spectra. For this purpose, one first has to minimize the energy of these QM fragments within their MM environments.

We have applied two protocols for the in situ minimizations of the quinones in *Rb. sphaeroides*. In a most simple approach, we have executed the minimization of the respective QM fragments in the frozen crystallographic structure. Here, the structures of the quinones are expected to be strongly influenced by the rigid shape of the binding pocket. In a second protocol, we have added a certain degree of flexibility. Here, we have also minimized the energy with respect to the coordinates of the protein side chains and of the remaining chromophores initially keeping the QM fragment and the protein backbone frozen. Subsequently, also the QM fragment was included into the minimization process and solely the backbone was kept fixed. We will refer to protein structures derived by this second minimization protocol as partially minimized structures. After minimization, the Hessian of the respective QM fragment was numerically computed by EGO/CPMD and a normal mode analysis was carried out as described in ref 11. This approach yields IR line spectra. The inhomogeneous broadening of IR lines, which is accessible through sampling of protein conformations obtained by room temperature MD simulation,[62,17] is neglected here. However, because an X-ray structure gives average atomic positions, the corresponding line spectra should be close to the centers of the broadened lines. Our second minimization protocol serves to check whether our force field is compatible with the X-ray structure: if the two line spectra are similar, one may assume compatibility.

3. Results and Discussion

Before presenting our results on the vibrational spectra of the ubiquinones in situ, we first have to clarify the quality of the DFT methods provided by CPMD for the description of

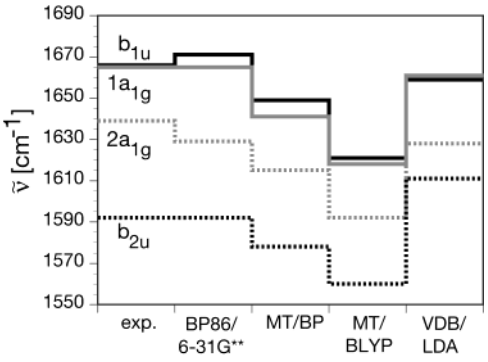

Figure 4. C═C and C═O modes of 1,4-benzoquinone calculated using various DFT methods. The experimental frequencies are those of Zhao et al.[63] For explanation and discussion, see the text.

quinone force fields. As indicated in the Introduction, for this purpose, we will compare CPMD results on vibrational modes of an isolated 1,4-benzoquinone molecule with those of our reference method BP86/6-31G**[34] and with experimental data.[63]

3.1. C═C and C═O Modes of 1,4-Benzoquinone. Figure 4 compares the C═O and C═C frequencies of 1,4-benzoquinone calculated by the MT/BP, MT/BLYP, and VDB/LDA methods offered by CPMD with the BP86/6-31G** results[34] and with the observations of Zhao et al.[63]

As mentioned above, the BP86/6-31G** calculation nicely reproduces the experimentally observed spectral positions of the C═O and C═C modes including their relative spacings. Therefore, these computational results will be taken as our reference for judging the quality of the results of the plane wave/pseudopotential calculations MT/BP, MT/BLYP, and VDB/LDA.

As compared to the reference, the vibrational frequencies predicted by MT/BP are homogeneously shifted toward lower frequencies by about 20 cm^{-1}. As a result of the homogeneity of shifting, the spectral spacings of the modes remain nearly invariant. Therefore, the observed band pattern can be explained equally well by the reference calculation and by the MT/BP results, if the uniform softening of spring constants in MT/BP is kept in mind. The force field of MT/BLYP is still softer than that of MT/BP as is witnessed by a further red shift of the corresponding band positions in Figure 4. Here, in addition, also the relative spectral spacings of the modes become sizeably smaller. At the first glance, the VDB/LDA results seem to agree better with experiment and with the reference calculation than those of the two other treatments. However, a closer inspection shows that this is actually not the case.

To provide arguments for this claim, consider Table 1, which lists the mode compositions of the four vibrations. These data show that the low-frequency b_{2u} mode is a pure C═C stretch, whereas the high-frequency b_{1u} mode is a pure C═O stretch according to all treatments. VDB/LDA shifts the b_{2u} C═C stretch by about 20 cm^{-1} to the blue and the b_{1u} C═O stretch by about 10 cm^{-1} to the red as compared to BP86/6-31G** and to the experimental data (cf. Figure 4). Thus, the method overestimates C═C and underestimates C═O force constants. Correspondingly, VDB/LDA describes the compositions of the two mixed a_{1g} modes quite differently as compared to the other treatments and the reference calculation. Whereas the reference and MT/BP unanimously assign a predominant C═O stretch character to the $1a_{1g}$ mode and a predominant C═C stretch character to the $2a_{1g}$ mode, this assignment becomes inverted already in the MT/BLYP treatment. According to VDB/LDA, this inversion is complete, since it assigns a nearly pure C═C character to $1a_{1g}$ and C═O character to $2a_{1g}$ (cf. Table 1). As a consequence of the similar mode compositions, also the isotope shifts upon complete ^{18}O or ^{13}C substitution are nearly identical for the reference[34] and MT/BP, whereas for MT/BLYP and VBD/LDA the different mode compositions entail other isotope shifting patterns (data not shown).

Thus, for identical BP functionals, the BP86/6-31G** and the MT/BP treatment give identical results, apart from a slight softening of spring constants in MT/BP. In contrast, the combinations MT/BLYP and VDB/LDA neither match the reference results nor the experimental data correspondingly well. Therefore, we will exclude these treatments from further consideration. Note, however, that for other purposes (e.g., for QM/MM MD simulations) the VDB/LDA force field may be accurate enough and, thus, may offer a cost effective alternative.

To facilitate future comparisons of experimental and of MT/BP frequencies, we have determined a scaling factor λ from a least-squares fit of scaled MT/BP results to the experimental data displayed in Figure 4. We have found the value $\lambda = 1.0122$ showing that MT/BP underestimates the observed frequencies by about 1%. As compared to the experimental data, the scaled MT/BP frequencies exhibit a root mean square (RMS) deviation of 2.5 cm^{-1}, whereas that of the reference method BP86/6-31G** is 3.7 cm^{-1}. Thus, scaled MT/BP reproduces the observations on 1,4-benzoquinone even better than unscaled BP86/6-31G**.

3.2. QM/MM Calculations of the Ubiquinones in *Rb. sphaeroides.* The calculation of the vibrational spectra of Q_A and Q_B requires an in situ QM/MM optimization of the structures of these compounds. Because the X-ray model[3] provides structural data, it seems worthwhile to carry out a structure comparison before turning to the analysis of FTIR data.

3.2.1. Structures of Q_A and Q_B. We characterize the structures of Q_A and Q_B by the orientations of the methoxy groups as measured by the dihedral angles τ_1 and τ_2 defined in Figure 2. According to the crystal structure, the two quinones have one methoxy group nearly in the ring plane ond the other one pointing out of plane at dihedral angles τ_1 and τ_2 of -4 and 116° for Q_A and of -110 and -16° for Q_B, respectively.

For Q_A, the QM/MM minimization in the frozen X-ray model predicts slightly different dihedrals at -18 and 119°, respectively. The added flexibility offered by our second minimization protocol leads to a prediction differing less from the X-ray model. Here, optimal values of -11 and 118° are found. As a result, the X-ray and the two QM/MM structures are quite similar in the case of Q_A.

For Q_B, however, drastic structural changes are obtained by our QM/MM minimizations. For the frozen protein model, we find dihedral angles of -149 and 40° indicating that the two methoxy groups have changed their orientations by -39 and 56°, respectively. Relaxing the strains exerted by the rigid binding pocket on Q_B yields dihedrals of -117 and 29°. Thus, in the partially minimized structures, the reorientations are smaller measuring -7 and 45°, respectively. Whereas for τ_1 the calculated -7° reorientation is compatible with the X-ray model, this is not the case for τ_2.

At this point, it is worthwhile to note that the temperature factors determined during crystallographic refinement are larger at Q_B than at Q_A implying that the 1PCR structure at Q_B has less support by the X-ray data than that at Q_A.[3] Correspondingly, an inspection of the crystallographic model reveals at Q_B a distorted quinone ring, whereas in our QM/MM structures the ring is nearly planar. Concerning the calculation of molecular structure, our QM/MM method should be extremely accurate.

TABLE 1: Total Energy Distributions of the C═C and C═O Stretching Modes of 1,4-Benzoquinone

	b_{1u}	$1a_{1g}$	$2a_{1g}$	b_{2u}
BP86/6-31G**[34]	88% C═O	55% C═O + 19% C═C	37% C═O + 56% C═C	83% C═C
MT/BP	88% C═O	50% C═O + 25% C═C	45% C═O + 50% C═C	75% C═C
MT/BLYP	86% C═O	28% C═O + 40% C═C	65% C═O + 34% C═C	74% C═C
VDB/LDA	86% C═O	12% C═O + 59% C═C	80% C═O + 17% C═C	76% C═C

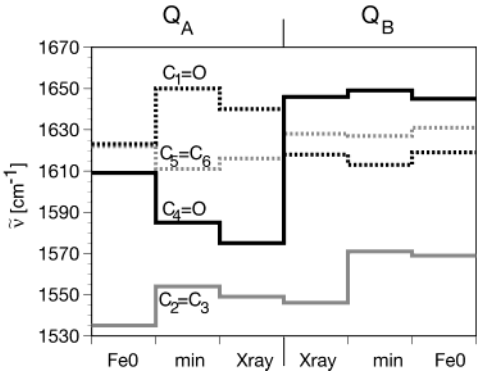

Figure 5. C═C and C═O modes of quinones QA and QB calculated in *Rb. sphaeroides* by our QM/MM approach with MT/BP. Xray, frozen X-ray structure; min, partially minimized RC structure; Fe0, partially minimized RC structure and uncharged iron cofactor.

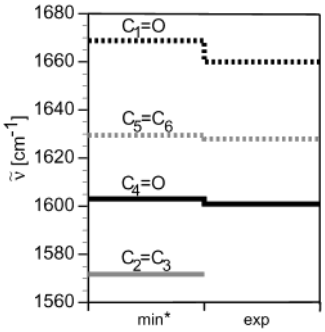

Figure 6. Comparison of experimental and calculated C═C and C═O modes of QA in *Rb. sphaeroides*. The QM/MM frequencies shown in the column min of Figure 5 have been scaled as explained in Section 3.1 and are now labeled by min*.

Therefore, this distortion must be an artifact of the crystallographic modeling. Because the distortion affects the dihedral angles τ_1 and τ_2, which we have computed from the X-ray structure, the quoted experimental values are not very reliable. On the other hand, our calculated dihedrals may be not very reliable either at Q_B, since several water molecules near Q_B may have been overlooked during the crystallographic refinement of the 1PCR structure and since we did not add possibly missing water molecules to that structure (cf. Section 2). Electrostatic interactions (e.g., hydrogen bridges) with such water molecules would change the structure of Q_B and, hence, also the outcome of our QM/MM structure calculations. Note in addition that other crystallographic models[64,65] localize Q_B at a different position within the RC of *Rb. sphaeroides*, which is closer to the iron cofactor. In summary, our structure calculations verify the X-ray model 1PCR for Q_A and confirm previous doubts on that for Q_B.

3.2.2. Vibrational Spectra of Q_A and Q_B. Now we are ready to address the central issue of this paper, which is the question, how the RC of *Rb. sphaeroides* steers the properties of the two ubiquinones. Our particular focus will be on the strong red shift of the C_4═O mode of Q_A[5,6] mentioned in the Introduction. Here, we have already indicated that this shift may be either due to the orientation of the methoxy groups[5,9] or, more likely, due to the electrostatic interactions of Q_A with the protein.[5,10,11,15] In the protein, the iron cofactor and the polar histidine M219 are possible interaction partners of Q_A and, therefore, might cause the red shift (cf. Figure 1).

The C═C and C═O frequencies of the two quinones as calculated in situ are presented in Figure 5. In addition, the figure displays the spectral effect of neutralizing the iron cofactor.

The most prominent feature in the term scheme displayed by Figure 5 is a C═O mode of Q_A calculated at low frequencies for the two structural models denoted by X-ray and min. This mode belongs to the stretching of the C_4═O bond, which in the RC is directed toward His M219 and the iron cofactor (cf. Figure 1). In the frozen X-ray structure, it is found 43 cm^{-1} to the red of the lower frequency C═O mode of Q_B, which belongs to the C_1═O stretch in this quinone. Adding flexibility by partial minimization renders a somewhat smaller but still sizable difference of 28 cm^{-1}. Hence, our QM/MM approach correctly predicts the C_4═O mode of Q_A at strongly red-shifted frequencies.

The remaining modes of Q_A and Q_B differ by less than than 10 cm^{-1}, if the results on the frozen X-ray structure are considered. The partial relaxation of the RC modifies the spectral positions of the modes at Q_A by at most 10 cm^{-1}, whereas in the case of Q_B, in line with its larger structural changes, its low-frequency C═C mode is strongly shifted to the blue.

To identify the mechanism for the red shift of the C_4═O mode at Q_A, we have also calculated the vibrational spectra of Q_A and Q_B with an uncharged iron atom. For this purpose, we have taken the partially minimized structure of the RC, have set the charge of the iron to zero, and have minimized the quinone keeping the RC structure fixed. The resulting term scheme of vibrational levels is denoted by Fe0 in Figure 5 and shows that neutralizing the iron cofactor causes a 24 cm^{-1} blue shift of the low-energy C_4═O mode of Q_A. As a result, this mode is found in the same spectral region as the corresponding mode of Q_B. The other vibrational frequencies of Q_A are also affected: the high-frequency C═O and the low-frequency C═C mode are both red-shifted by 27 and 21 cm^{-1}, respectively. At Q_B, in contrast, the neutralization of the iron cofactor has only a very small influence on the vibrational spectrum entailing shifts of at most 6 cm^{-1}.

Thus, our calculations demonstrate that the RC of *Rb. sphaeroides* modifies the force field of Q_A by means of the electrostatic field, which is generated by the iron cofactor, acts on Q_A, and shifts its C_4═O frequency to the red. This result could be considered as hard evidence, if the vibrational frequencies calculated for Q_A should quantitatively match the corresponding FTIR data. To carry out such a quantitative comparison, we will use the scaling factor $\lambda = 1.0122$, which we have derived in Section 3.1 exactly for this purpose.

Figure 6 quantitatively compares FTIR data on Q_A[5,10] with our scaled QM/MM results obtained for the partially relaxed RC. The agreement is obviously excellent. The RMS deviation measures 4.6 cm^{-1} and is similarly small as the one found in Section 3.1 for 1,4-benzoquinone, where we have compared vacuum DFT descriptions with gas phase IR data. The nearly perfect match of the observed and the calculated Q_A frequencies now demonstrates that our QM/MM approach can yield equally

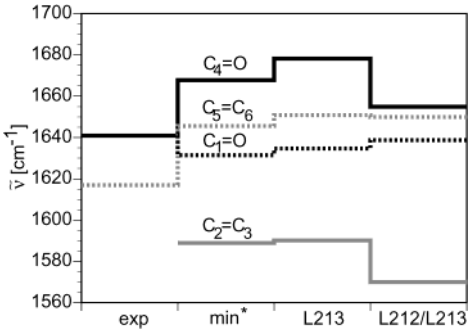

Figure 7. Comparison of experimental and calculated C═C and C═O modes of QB in *Rb. sphaeroides*. The QM/MM frequencies shown in the column min of Figure 5 have been scaled as explained in Section 3.1 and are now labeled by min*. The columns L213 and L213/L212 refer to RC structures minimized with ionized residues. For further explanation, see the text.

accurate descriptions of vibrational spectra also for molecules in condensed phase, if a correct model for the structure of the environment is available. Motivated by our experience with the sensitivity and accuracy of such QM/MM force field calculations,[16,17] we even go one step further and claim that conversely, the agreement of calculated and observed FTIR band positions represents a proof for the correctness of a structural model. Applying this claim to the 1PCR structure suggests that it is correct in the surroundings of Q_A. This conclusion is supported by the comparison of the observed and the calculated Q_A structures presented further above, which had also shown a close agreement. However, because molecular structures use to be much less sensitive probes on influences of the environment than vibrational spectra, we did not consider the favorable outcome of the structure comparison as hard evidence.

The above claims are corroborated by the results of similar calculations on the light-adapted 1DV3 structure of Stowell et al.,[53] which we intend to publish in detail elsewhere. Here, the computed Q_A frequencies agree extremely well with the data presented above (RMS deviation: 9 cm^{-1}) whereas for Q_B substantial differences are found. The latter differences are due to different structures of the Q_B binding pockets. The agreement concerning the Q_A IR spectra is in line with the similarity of the Q_A binding pockets in 1PCR and 1DV3.

As a corollary of the perfect description of the Q_A bands by our QM/MM approach, we now can safely conclude that the low-frequency position of the C_4═O mode is due to the electric field generated by the iron cofactor. This field can exert such a strongly polarizing influence on Q_A, because the C_4═O bond points directly toward the iron (cf. Figure 1).

In the case of Q_B, the calculated and the observed frequencies shown in Figure 7 exhibit strong differences. According to the FTIR data on Q_B,[4,66] there is only one C═O mode at 1641 cm^{-1} carrying IR intensity. This indicates that the two C═O force constants are nearly degenerate in Q_B, that symmetric and antisymmetric combinations are formed, and that only the latter carries intensity. Similarly, only one C═C band has been detected at 1617 cm^{-1}. In contrast, our QM/MM calculation predicts one C═O mode for each carbonyl bond. Here, the high-frequency C_4═O mode is an almost pure carbonyl stretch, whereas the lower frequency C_1═O mode is strongly mixed with the C_5═C_6 stretch. The frequencies calculated for the two carbonyl stretching modes deviate by 30 and 10 cm^{-1}, respectively, from the spectral position of the observed band. Similarly large deviations are found in the case of the C═C modes.

These deviations show that our model of the 1PCR structure used for the calculation and denoted as min* in Figure 7 is incompatible with the FTIR data. However, there is only one essential ambiguity distinguishing the 1PCR structure from our model, which is the protonation state of Glu L212 and Asp L213 in the vicinity of Q_B. Because the X-ray structure does not provide any clue to this problem and because other clear evidence is lacking (cf. Section 2), we had to fix a particular choice for our calculation, which was to choose both acids to be protonated. To check whether other protonation patterns lead to calculated spectra, which are compatible with the FTIR data, we have first deprotonated Asp L213 and, subsequently, also Glu L212. The resulting QM/MM spectra are also shown in Figure 7. Deprotonation of L213 scarcely affects the Q_B spectrum. The additional deprotonation of L212 leads to the protonation state predicted by the calculations of Sham et al.[60] and induces strong red shifts of the C_4═O and C_2═C_3 modes as well as a slight blue shift of the C_1═O stretch. As far as the two C═O modes are concerned, these spectral changes diminish the differences to the observations. However, for the C═C modes, sizable differences remain. They are too large as to be compatible with the FTIR data. Thus, it is the 1PCR structure itself that is incompatible with FTIR.

Of course, one can speculate a lot about possible reasons for this incompatibility. It may be, for instance, that under the experimental conditions of the FTIR measurements the RC actually has a structure near Q_B different from that in the crystal. It may also be that the water molecules most likely missing in the X-ray structure (cf. Section 2) could repair the incompatibility. For a check, one would have to add water molecules to the structure, determine their equilibrium distribution by MD simulation, and calculate IR spectra for various cases. Furthermore, it may be that the 1PCR structure localizes Q_B at a wrong position within the RC. We cannot decide on these issues on the basis of our calculations. All we can state is that the 1PCR structure is incompatible with FTIR as far as Q_B is concerned and that it is now proven to be correct near Q_A.

4. Summary and Outlook

Using the ubiquinones Q_A and Q_B of the bacterial photosynthetic RC of *Rb. sphaeroides* as our testing ground, we have shown that advanced QM/MM methods allow in situ calculations of vibrational spectra, which exhibit a quality comparable to that of previous vacuum calculations on gas phase spectra. When combined with FTIR data, the computational results are accurate enough as to allow us judgments on the quality of a given X-ray model. If the X-ray model is correct, the calculated vibrational spectrum of a prosthetic group should match the FTIR observations within the margins of a few cm^{-1}. If no such agreement can be achieved, one can safely conclude that the X-ray structure and the FTIR data are incompatible.

Applying this strategy to the ubiquinones Q_A and Q_B in the structure 1PCR[3] of the RC of *Rb. sphaeroides*, we have shown that this structure is correct at Q_A and incompatible with FTIR at Q_B. The calculations reproduce the low-frequency position of the C_4═O mode of Q_A and demonstrate that the electric field of the iron cofactor is responsible for this unusual red shift. For Q_B, no structural conclusions can be derived from the calculations and from their comparison with the quoted FTIR data.

Having thus established an approach to the in situ computation of vibrational spectra for protein cofactors, new problems may be addressed. In our study, the protein structures entering the QM/MM modeling had been chosen very close to the X-ray data. In cases in which the FTIR and X-ray data are found to be incompatible, one could now try, for instance, to use

molecular modeling and MD simulation techniques to determine a better structure. Furthermore, one should apply the approach to cases well-studied by FTIR like the retinal chromophore of bacteriorhodopsin (see, e.g., ref 67 and references quoted therein) or the guanosin triphosphate in the G-protein *Ras* P21[68] in order to get further structural insights into these proteins.

Acknowledgment. This work was supported by the Volkswagenstiftung (Project I/73 224) and by the Deutsche Forschungsgemeinschaft (SFB533/C3). Computer time was provided by the Leibniz-Rechenzentrum (Project h0431). M.N. thanks Jacques Breton and Eliane Nabedryk for numerous enlightening and highly motivating discussions about photosynthetic RCs and vibrational spectra of quinones during the past decade.

References and Notes

(1) Trumpower, B. L. *Function of Quinones in Energy Conservation*; Academic Press: New York, 1982.
(2) Okamura, M. Y.; Paddock, M. L.; Graige, M. S.; Feher, G. *Biochim. Biophys. Acta* **2000**, *1458*, 148−163.
(3) Ermler, U.; Fritzsche, G.; Buchanan, S. K.; Michel, H. *Structure* **1994**, *2*, 925−936.
(4) Breton, J.; Boullais, C.; Berger, G.; Mioskowski, C.; Nabedryk, E. *Biochemistry* **1995**, *34*, 11606.
(5) Brudler, R.; de Groot, H. J. M.; van Liemt, W. B. S.; Steggerda, W. F.; Esmeijer, R.; Gast, P.; Hoff, A. J.; Lugtenburg, J.; Gerwert, K. *EMBO J.* **1994**, *13*, 5523.
(6) Breton, J.; Burie, J.-R.; Boullais, C.; Berger, G.; Nabedryk, E. *Biochemistry* **1994**, *33*, 12405.
(7) Mancino, L. J.; Dean, D. P.; Blankenship, R. E. *Biochim. Biophys. Acta* **1984**, *764*, 46−54.
(8) Kleinfeld, D.; Okamura, M. Y.; Feher, G. *Biochim. Biophys. Acta* **1984**, *766*, 126.
(9) Burie, J.-R.; Boullais, C.; Nonella, M.; Mioskowski, C.; Nabedryk, E.; Breton, J. *J. Phys. Chem. B* **1997**, *101*, 6607.
(10) Breton, J.; Boullais, C.; Burie, J.-R.; Nabedryk, E.; Mioskowski, C. *Biochemistry* **1994**, *33*, 14378−14386.
(11) Nonella, M.; Brändli, C. *J. Phys. Chem.* **1996**, *100*, 14549.
(12) Robinson, H. H.; Kahn, S. D. *J. Am. Chem. Soc.* **1990**, *112*, 4728.
(13) Nonella, M. *J. Phys. Chem. B* **1998**, *102*, 4217.
(14) Nonella, M. *Photosynth. Res.* **1998**, *55*, 253.
(15) Nonella, M.; Boullais, C.; Mioskowski, C.; Nabedryk, E.; Breton, J. *J. Phys. Chem. B* **1999**, *103*, 6363−6370.
(16) Eichinger, M.; Tavan, P.; Hutter, J.; Parrinello, M. *J. Chem. Phys.* **1999**, *110*, 10452−10467.
(17) Eichinger, M. Berechnung molekularer Eigenschaften in komplexer Lösungsmittelumgebung: Dichtefunktionaltheorie kombiniert mit einem Molekularmechanik-Kraftfeld, Thesis, Ludwig-Maximilians Universität München, Germany, 1999.
(18) Warshel, A.; Levitt, M. *J. Mol. Biol.* **1976**, *103*, 227−249.
(19) Hohenberg, P.; Kohn, W. *Phys. Rev.* **1964**, *136*, B864−B870.
(20) Kohn, W.; Sham, L. J. *Phys. Rev.* **1965**, *140*, A1133−A1138.
(21) Stanton, R. V.; Hartsough, D. S.; Merz, K. M. *J. Phys. Chem.* **1993**, *97*, 11868.
(22) Svenssons, M.; Humbel, S.; Froese, R. D. J.; Matsubara, T.; Sieber, S.; Morokuma, K. *J. Phys. Chem.* **1996**, *100*, 19357.
(23) Matsubara, T.; Maseras, F.; Koga, N.; Morokuma, K. *J. Phys. Chem.* **1996**, *100*, 2573.
(24) Tuñón, I.; Martins-Costa, M. T. C.; Millot, C.; Ruiz-López, M. F.; Rivail, J. L. *J. Comput. Chem.* **1996**, *17*, 19.
(25) Tuñón, I.; Martins-Costa, M. T. C.; Millot, C.; Ruiz-López, M. F. *J. Chem. Phys.* **1997**, *106*, 3633.
(26) Strnad, M.; Martins-Costa, M. T. C.; Millot, C.; Tuñón, I.; Ruiz-López, M. F.; Rivail, J. L. *J. Chem. Phys.* **1997**, *106*, 3643.
(27) Hutter, J.; Alavi, A.; Deutsch, T.; Bernasconi, M.; Goedecker, S.; Marx, D.; Tuckermann, T.; Parrinello, M. *CPMD* Version 3.4.0; MPI für Festkörperforschung and IBM Zurich Research Laboratory.
(28) Niedermeier, C.; Tavan, P. *J. Chem. Phys.* **1994**, *101*, 734.
(29) Niedermeier, C.; Tavan, P. *Mol. Simul.* **1996**, *17*, 57−66.
(30) Eichinger, M.; Grubmüller, H.; Heller, H.; Tavan, P. *J. Comput. Chem.* **1997**, *18*, 1729.
(31) Mathias, G.; Egwolf, B.; Nonella, M.; Tavan, P. Manuscript in preparation.
(32) Frisch, M. J.; et al. *Gaussian 98*, Revision A.5; Gaussian, Inc.: Pittsburgh, PA, 1999.
(33) Zhou, X.; Mole, S. J.; Liu, R. *Vib. Spectrosc.* **1996**, *12*, 73−79.
(34) Nonella, M.; Tavan, P. *Chem. Phys.* **1995**, *199*, 19.
(35) Becke, A. D. *Phys. Rev. A* **1988**, *38*, 3098.
(36) Perdew, J. P. *Phys. Rev. B* **1986**, *33*, 8822.
(37) Francl, M.; Pietro, W.; Hehre, W.; Binkley, J.; Gordon, M.; deFrees, D.; Pople, J. *J. Chem. Phys.* **1982**, *77*, 3654.
(38) Boesch, S. E.; Wheeler, R. A. *J. Phys. Chem.* **1995**, *99*, 8125.
(39) Boesch, S. E.; Wheeler, R. A. *J. Phys. Chem. A* **1997**, *101*, 5799−5804.
(40) Himo, F.; Babcock, G. T.; Eriksson, L. A. *J. Phys. Chem. A* **1999**, *103*, 3745−3749.
(41) Nilsson, J. A.; Lyubartsev, A.; Eriksson, L. A.; Laaksonen, A. *Mol. Phys.* **2001**, *99*, 1795−1804.
(42) Troullier, N.; Martins, J. *Phys. Rev. B* **1991**, *43*, 1993.
(43) Lee, C.; Yang, W.; Parr, R. C. *Phys. Rev. B* **1988**, *37*, 785.
(44) Laasonen, K.; Sprik, M.; Parrinello, M.; Car, R. *J. Chem. Phys.* **1993**, *99*, 9081.
(45) Vanderbilt, D. *Phys. Rev. B* **1990**, *41*, 7892.
(46) Parr, R. G.; Yang, W. *Density-Functional Theory of Atoms and Molecules*; Oxford University Press: New York, 1989.
(47) Brooks, B. R.; Bruccoleri, R. E.; Olafson, B. D.; States, D. J.; Swaminathan, S.; Karplus, M. *J. Comput. Chem.* **1983**, *4*, 187.
(48) Treutlein, H.; Schulten, K.; Deisenhofer, J.; Michel, H.; Brünger, A.; Karplus, M. Molecular Dynamics Simulation of the Primary Processes in the Photosynthetic Reaction Center of Rhodpseudomonas viridis. In *The Photosynthetic Bacterial Reaction Center*; Breton, J., Vermeglio, A., Eds.; Plenum Publishing Corporation: New York, 1988; Vol. 149.
(49) Treutlein, H. Molekulardynamiksimulation des photosynthetischen Reaktionszentrums von Rhodopseudomonas viridis, Thesis, Technische Universität München, Germany, 1988.
(50) Nonella, M.; Schulten, K. *J. Phys. Chem.* **1991**, *95*, 2059.
(51) Hutter, M. C.; Hughes, J. M.; Reimers, J. R.; Hush, N. S. *J. Phys. Chem. B* **1999**, *103*, 4906−4915.
(52) Brünger, A. T. Crystallographic refinement by simulated annealing. In *Crystallographic Computing 4*: *Techniques and New Technologies*; Isaacs, N. W., Taylor, M. R., Eds.; Clarendon Press: Oxford, 1988.
(53) Stowell, M. H. B.; McPhillips, T. M.; Rees, D. C.; Soltis, S. M.; Abresch, E.; Feher, G. *Science* **1997**, *276*, 812−816.
(54) Paddock, M. L.; Feher, G.; Okamura, M. Y. *Biochemistry* **1997**, *36*, 14238−14249.
(55) Alexov, E. G.; Gunner, M. R. *Biochemistry* **1999**, *38*, 8253−8270.
(56) Rabenstein, B.; Ullmann, G. M.; Knapp, E.-W. *Biochemistry* **2000**, *39*, 10487−10496.
(57) Nabedryk, E.; Breton, J.; Hienerwadl, R.; Fogel, C.; Mäntele, W.; Paddock, M. L.; Okamura, M. Y. *Biochemistry* **1995**, *34*, 14722−14732.
(58) Walden, S. E.; Wheeler, R. A. *J. Phys. Chem. B* **2002**, *106*, 3001−3006.
(59) Sham, Y. Y.; Muegge, I.; Warshel, A. *Biophys. J.* **1998**, *74*, 1744−1753.
(60) Sham, Y. Y.; Muegge, I.; Warshel, A. *Proteins*: *Struct., Funct., Genet.* **1999**, *36*, 484−500.
(61) Breton, J.; Nabedryk, E.; Allen, J. P.; Williams, J. C. *Biochemistry* **1997**, *36*, 4515−4525.
(62) Bentzien, J.; Muller, R. P.; Florián, J.; Warshel, A. *J. Phys. Chem. B* **1998**, *102*, 2293−2301.
(63) Zhao, X.; Imahori, H.; Zhan, C.-G.; Mizutani, Y.; Sakata, Y.; Kitagawa, T. *Chem. Phys. Lett.* **1996**, *262*, 643.
(64) Allen, J. P.; Feher, G.; Yeates, T. O.; Komiya, H.; Rees, D. C. *Proc. Natl. Acad. Sci. U.S.A.* **1988**, *85*, 8487−8491.
(65) El-Kabbani, O.; Chang, C.-H.; Tiede, D.; Norris, J.; Schiffer, M. *Biochemistry* **1991**, *30*, 5361−5369.
(66) Brudler, R.; de Groot, H. J. M.; van Liemt, W. B. S.; Gast, P.; Hoff, A. J.; Lugtenburg, J.; Gerwert, K. *FEBS Lett.* **1995**, *370*, 88−92.
(67) Grossjean, M. F.; Tavan, P.; Schulten, K. *J. Phys. Chem.* **1990**, *94*, 8059.
(68) Allin, C.; Gerwert, K. *Biochemistry* **2001**, *40*, 3037−3046.